HHS Public Access

Author manuscript

J Mol Cell Cardiol. Author manuscript; available in PMC 2023 May 25.

Published in final edited form as:

J Mol Cell Cardiol. 2022 September ; 170: 34–46. doi:10.1016/j.yjmcc.2022.05.009.

Dual loss of regulator of G protein signaling 2 and 5 exacerbates ventricular myocyte arrhythmias and disrupts the fine-tuning of $G_{i/o}$ signaling

Shelby A. Dahlen[a], **Tyler F. Bernadyn**[b], **Alethia J. Dixon**[a], **Bo Sun**[a], **Jingsheng Xia**[a], **Elizabeth A. Owens**[b], **Patrick Osei-Owusu**[a,b,*]

[a]Department of Physiology & Biophysics, Case Western Reserve University School of Medicine, Cleveland, OH 44106, United States of America

[b]Department of Pharmacology & Physiology, Drexel University College of Medicine, Philadelphia, PA 19102, United States of America

Abstract

Aims: Cardiac contractility, essential to maintaining proper cardiac output and circulation, is regulated by G protein-coupled receptor (GPCR) signaling. Previously, the absence of regulator of G protein signaling (RGS) 2 and 5, separately, was shown to cause G protein dysregulation, contributing to modest blood pressure elevation and exaggerated cardiac hypertrophic response to pressure-overload. Whether RGS2 and 5 redundantly control G protein signaling to maintain cardiovascular homeostasis is unknown. Here we examined how the dual absence of RGS2 and 5 (*Rgs2/5* dbKO) affects blood pressure and cardiac structure and function.

Methods and results: We found that *Rgs2/5* dbKO mice showed left ventricular dilatation at baseline by echocardiography. Cardiac contractile response to dobutamine stress test was sex-dependently reduced in male *Rgs2/5* dbKO relative to WT mice. When subjected to surgery-induced stress, male *Rgs2/5* dbKO mice had 75% mortality within 72–96 h after surgery, accompanied by elevated baseline blood pressure and decreased cardiac contractile function. At the cellular level, cardiomyocytes (CM) from *Rgs2/5* dbKO mice showed augmented Ca^{2+} transients and increased incidence of arrhythmia without augmented contractile response to electrical field stimulation (EFS) and activation of β-adrenergic receptors (βAR) with isoproterenol. Dual loss of *Rgs2* and 5 suppressed forskolin-induced cAMP production, which was restored by $G_{i/o}$ inactivation with pertussis toxin that also reduced arrhythmogenesis during EFS or βAR stimulation. Cardiomyocyte NCX and PMCA mRNA expression was unaffected in *Rgs2/5*

*Corresponding author at: Case Western Reserve University School of Medicine, Physiology & Biophysics Department, 10900 Euclid Avenue Robbins E526, Cleveland, OH 44106, United States of America. pxo70@case.edu (P. Osei-Owusu).

Author contributions

PO-O conceived and designed the study; SAD, TFB, AD, BS, JX, EAO, and PO-O performed experiments, analyzed data, contributed to the revision of manuscript; PO-O drafted, edited, revised, and approved the final version of the manuscript.

Declaration of Competing Interest

None declared.

Supplementary data to this article can be found online at https://doi.org/10.1016/j.yjmcc.2022.05.009.

dbKO male mice. However, there was an exaggerated elevation of EFS-induced cytoplasmic Ca^{2+} in the presence of SERCA blockade with thapsigargin.

Conclusions: We conclude that RGS2 and 5 promote normal ventricular rhythm by coordinating their regulatory activity towards $G_{i/o}$ signaling and facilitating cardiomyocyte calcium handling.

Keywords

RGS proteins; G protein signaling; Cardiac excitation-contraction coupling; Arrhythmia; Cardiomyopathy; cAMP; Catecholamine

1. Introduction

Signaling downstream of heterotrimeric G proteins mediates the effects of several endogenous stimuli and G protein-coupled receptor (GPCR) agonists, including catecholamines, on cardiac structure and function. Aberrant G protein signaling is implicated in the pathogenesis of cardiac disorders including maladaptive hypertrophy leading to heart failure, and arrhythmias. Accordingly, pharmacological targeting of cardiac GPCR and their effectors is an established therapeutic approach to managing various cardiac disorders including ventricular arrhythmias and heart failure [1].

G protein signaling is fine-tuned by regulator of G protein signaling (RGS) proteins [2]. RGS proteins are GTPase activating proteins (GAPs) that accelerate the hydrolysis of GTP to GDP by the intrinsic GTPase activity of the Gα subunit. In so doing, RGS proteins facilitate the termination of signaling by regulating the magnitude and duration of G protein activity [3]. RGS proteins are widely expressed in vertebrates. In the heart, several members of the B/R4 family, including RGS1–5, 8, 13, 16, and 18 are expressed, at least at the mRNA level [4,5]. RGS proteins of the B/R4 family act as GAPs towards $G_{q/11}$ and $G_{i/o}$ class G proteins. Among this family of RGS proteins, RGS2 and RGS5 are most noted for regulating β_2-adrenergic receptor (β_2AR)-mediated $G\alpha_{i/o}$ signaling within the myocardium [6-8]. In cardiomyocytes, the overexpression of RGS2 suppresses agonist-induced, β_2AR-mediated $G_{\alpha i}$ signaling, a pathway implicated in ventricular arrhythmia, heart failure, and hypertension [7]. Similar to RGS2, RGS5 has also been shown to display relevance in proper cardiac function, specifically in the repolarization phase of cardiac contraction [9,10], hypertrophy and fibrosis [11,12], and maintenance of blood pressure homeostasis [13]. Thus, RGS2 and 5 seem to play overlapping roles in the cardiovascular system. However, it is unclear whether RGS2 and 5 redundantly control G protein signaling to maintain homeostasis in the cardiovascular system. To fill this knowledge gap, we generated mice dually lacking RGS2 and 5 (*Rgs2/5* dbKO).

In this study, we determined whether RGS2 and RGS5 show any compensatory or synergistic relationship in their regulation of cardiac structure and function. We report that *Rgs2/5* dbKO mice develop spontaneous left ventricular dilatation in the absence of an experimental stressor. In addition, *Rgs2/5* dbKO male mice are less responsive to βAR stimulation but are highly sensitive and succumb to surgery-related stress. Furthermore, the dual absence of RGS2 and 5 increases the susceptibility of ventricular myocytes

to arrhythmias following βAR stimulation or pacing by electrical field stimulation, by mechanisms involving increased $G\alpha_{i/o}$ activity and impaired cytoplasmic calcium handling.

2. Methods

2.1. Animal models

The generation of *Rgs2* and *Rgs5* null mice (*Rgs2*$^{-/-}$ *or Rgs2* KO and *Rgs5*$^{-/-}$ *orRgs5* KO) has been described previously [14,15]. The *Rgs2* KO mouse model was obtained from Dr. Kendall Blumer at Washington University, with permission from Dr. Josef Penninger, while *Rgs5* KO mice were obtained from Dr. John Kehrl at the NIH-NIAID. Both mouse lines have been backcrossed extensively into the C57BL/6 genetic background [15,16]. We performed *Rgs2*$^{-/-}$ x *Rgs5*$^{-/-}$ crosses to generate *Rgs2*$^{-/-}$,*Rgs5*$^{+/-}$; *Rgs2*$^{+/-}$,*Rgs5*$^{-/-}$; and *Rgs2*$^{+/-}$,*Rgs5*$^{+/-}$ mouse lines. We then crossed *Rgs2*$^{+/-}$,*Rgs5*$^{+/-}$ mice to generate mice dually null for *Rgs2* and 5 (*Rgs2/5* dbKO). The Institutional Animal Care and Use Committees at Drexel University and Case Western Reserve University approved the protocols for all animal experiments performed in this study, in accordance with the U.S. animal welfare act. We used 2- to 5-month-old male and female mice in all experiments involving adult animals. The mice were provided access to food and water ad libitum in our institution's animal facility at 22 °C and a 12-h light/dark cycle.

2.2. Conscious hemodynamics and ECG monitoring by radiotelemetry

Blood pressure, heart rate, and cardiac electrocardiogram (ECG) were measured in conscious wild type (WT) and *Rgs2/5* dbKO male and female mice using radiotelemetry, as we have previously described [17]. For conscious blood pressure measurement, HD-X10 radiotelemetry catheters and transmitters were implanted, as we have previously described [18]. Using Ponemah data acquisition system from Data Science International, recording of diurnal blood pressure and heart rate of conscious mice was initiated on day zero, i.e., immediately after the mice recovered from isoflurane anesthesia for the implantation of the radiotelemetry catheter. The acquired data were reduced to averages of continuous systolic blood pressure (SBP), diastolic pressure (DBP), mean blood pressure (MBP), and heart rate recordings in one-hour intervals over 24 h for 10 days, or until the mice died. For ECG monitoring, we used HD-X11 radiotelemeter implants. The mice were allowed to recover for at least one week from the transmitter implantation surgery prior to initiating recordings.

2.3. Echocardiography

All imaging studies were performed using Vevo 2100 cardiac echocardiography system equipped with a 400-MHz linear transducer (VisualSonics Inc., Toronto, Canada). Mice were lightly anesthetized with isoflurane (1.5%) and placed supine on a heated pad equipped with ECG electrodes for continuous monitoring throughout the imaging procedure. After the chest hair was removed with hair removal cream, two-dimensional parasternal long- and short-axis views at the midventricular level, as well as 1-dimensional targeted M-mode tracings throughout the anterior and posterior LV walls were recorded, as previously described [19,20]. The reported data are mean values obtained from at least 6 mice of each group and analyzed for statistical significance by ANOVA or Student's *t*-test, where appropriate.

2.4. Cardiac stress test and monitoring by echocardiography

Adult male and female mice were secured on a heated pad for echocardiography, as described above. A working solution of dobutamine hydrochloride (DOB, 10 μg/μl) was prepared from DOB stock (1 g/ml in DMSO) in 1:100 dilution in normal saline. After baseline recordings, the mice received intraperitoneal infusion of DOB (5 μg/kg/ min) for 1 min, using an infusion pump, as previously described [21]. Changes in left ventricular M-mode fractional shortening, in response to the infusion, were calculated offline.

2.5. Assessment of baseline cardiac function by pressure-volume loop analysis

We examined cardiac hemodynamics in isoflurane-anesthetized mice using closed-chest pressure-volume loop approach, as previously described [22]. Briefly, a 1.4F pressure-volume (PV) catheter (SPR 839; Millar Instruments, Inc.) was inserted into the right carotid artery and advanced past the aortic valve to lie longitudinally in the left ventricle. The mice were allowed to stabilize for 5 min while the isoflurane anesthetic was lowered from 3 to 1.5%. Data were acquired at baseline and during momentary occlusion of the inferior vena cava by compression of the abdomen with a dry cotton-tipped applicator. Shortly after the occlusion, a PE-10 catheter was placed in the right jugular vein for saline injection. Using a 1/3 cc insulin syringe, 10 μl of 20% saline was injected via the jugular vein for catheter calibration. At the end of the hemodynamics recording, blood was drawn for absolute volume calibration, according to the manufacturer's protocol. Throughout the experiment, data were acquired at 1KHz and analyzed using Labchart 8.0 software (ADInstruments). We used 10–15 PV loops to calculate stroke work, cardiac output, stroke volume, arterial elastance, and relaxation time constant. End-systolic PV relation (a.ka. end-systolic elastance) was calculated from the slope of PV loops acquired during momentary vena cava occlusion.

2.6. Isoproterenol (ISO)- and exercise-induced stress tests with simultaneous monitoring of hemodynamics and ECG

This test employed only male mice. After the acquisition of baseline blood pressure (BP), heart rate, and ECG for 30 min, the mice received a bolus injection of ISO (0.75 μg/g, i.p.) and returned to their home cages, with continuous ECG and BP monitoring for 60 min. A day after the acute ISO injection, and following 30 min of baseline recordings, the mice were placed in 4-l beaker containing 1.2 l of pre-warmed water to initiate a 90-min forced swimming, with continuous recording of hemodynamics and ECG. An extra 30 min of data acquisition was obtained when the mice were returned to their home cages at the end of the forced-swim test.

2.7. RNA isolation and gene expression analysis by real-time polymerase chain reaction

Total RNA was extracted from heart apexes of male and female WT and *Rgs2/5 dbKO mice* via a Trizol extraction method (ThermoFisher Scientific) and utilizing an Omni Bead Ruptor 24 homogenizer (Omni International) with tissue homogenizer tubes. RNA was purified using the Purelink RNA Mini Kit (ThermoFisher) and then reverse-transcribed using a Maxima First Strand cDNA Synthesis Kit (ThermoFisher Scientific), all according to the manufacturer's instructions. The primer probes listed in Table S4 were used in the

real-time PCR assays with TaqMan gene expression master mix (ThermoFisher Scientific): The ΔC_t method (where C_t is threshold cycle) was used to calculate mRNA expression after normalization to *Gapdh* expression.

2.8. Isolation and preparation of left ventricular cardiomyocytes from adult mouse hearts

Single cardiomyocytes were isolated using a simplified, Langendorff-free method adopted from Matthew Ackers-Johnson et al. [23]. EDTA buffer containing (in mM) 130 NaCl, 5 KCl, 0.5 NaH_2PO_4, 10 HEPES, 10 glucose, 10 BDM (Sigma-Aldrich), 10 Taurine, and 5 EDTA (pH 7.8 with NaOH) was prepared and stored at 4 °C up to two weeks. Perfusion buffer containing (in mM) 130 NaCl, 5 KCl, 0.5 NaH_2PO_4, 10 HEPES, 10 glucose, 10 BDM, 10 taurine, and 1 $MgCl_2$ (pH 7.8 with NaOH) was prepared and stored at 4 °C fridge up to two weeks. Collagenase buffer containing 0.5 mg/ml collagenase type 2, 0.5 mg/ml collagenase type 4 (Worthington Biochemical Corporation), and 0.05 mg/ml protease XIV (Sigma-Aldrich) was prepared the day of the isolation. Stop buffer was made with 5% FBS in perfusion buffer on the day of isolation. Mice were anesthetized using isoflurane, and the chest was opened to expose the heart. Seven ml EDTA buffer was perfused into the right ventricle. The ascending aorta was clamped using a Ductus clamp, and the heart was removed by cutting behind the clamp. The heart was transferred into a 30-mm dish containing EDTA buffer and then perfused with another 10 ml EDTA through the left ventricle. The heart was transferred into another 30-mm dish containing perfusion buffer and perfused with 3 ml perfusion buffer through the left ventricle. The heart was then transferred into another 30-mm dish containing collagenase buffer and perfused with 30 ml collagenase buffer for at least 15 min. The excess tissue including the right ventricle, atria, etc. were excised. The remaining left ventricle was transferred to another 30 mm dish containing about 5 ml collagenase buffer and was gently separated into 1 mm pieces using forceps, before being drawn up into a 1 ml pipette tip with the tip cut to ensure a larger opening. The 1 mm pieces of tissue were drawn up and down the pipette tip for about 2 min. Five ml of stop buffer was added to the 30 mm dish, and the pieces of tissue were drawn up and down the pipette again for about a minute. The cell suspension was passed through a 100-μm filter into a 50 mL conical tube, and the filtered suspension was transferred to a 15-ml conical tube. Cells underwent 3 sequential rounds of Ca^{2+} reintroduction (0.2, 0.5, and 1 mM) in perfusion buffer by gravity settling for 15–20 min/round and were stored in perfusion buffer with 1 mM Ca^{2+} at room temperature until use.

2.9. Simultaneous measurement of Ca^{2+} transients and contractility in cardiomyocyte

Isolated cardiomyocytes were loaded with 10 μM Fluo-4 AM (Fisher Scientific) and 0.02% Pluronic F-127 (Life Technologies) for 20 min at room temperature in 1 mM Ca^{2+} perfusion buffer. Cells were centrifuged (rcf 50 x*g* for 2 min) at room temperature and resuspended in Tyrode's solution containing (in mM) 140 NaCl, 5 KCl, 2 $CaCl_2$, $MgCl_2$, 10 HEPES, and 5.6 glucose (adjusted to pH 7.36 with NaOH). Cells were then transferred into a glass-bottom chamber mounted on the stage of an inverted microscope (Nikon Eclipse T*i*). Calcium transients and contractility in single cardiomyocytes were recorded with IonOptix excitation-contraction coupling data acquisition system (IonOptix LLC, MA). After settling on the glass coverslip, cells were continuously perfused with Tyrode's solution at a flow rate of 1.8 ml/min and paced with electric field stimulation (EFS) at 10 V voltage, 0.5 Hz

throughout the experiment. After baseline recording, cardiomyocytes were perfused with the non-selective βAR agonist, isoproterenol (ISO, Sigma-Aldrich) at increasing concentrations (10^{-8} to 10^{5} M) in Tyrode's solution via a pump. Cardiomyocyte Ca^{2+} transients and contractile properties were analyzed using IonOptix data processing software. ISO-induced arrhythmic activity including premature ventricular contractions, tachycardia, and temporary pause were judged by both Ca^{2+} transient and contractility traces, and the incidence of arrhythmic activity in response to ISO was counted before and after the application of each concentration of ISO.

2.10. Measurement of forskolin-stimulated cAMP production in freshly isolated adult ventricular cardiomyocytes

Following 20 min of incubation in Tyrode buffer containing 500 μM 3-isobutyl-1-methylxannthine (IBMX), freshly isolated left ventricular cardiomyocytes were stimulated at 37 °C for 5 min with vehicle or forskolin (1, 10, or 50 μM) in the absence or presence of the (α_2-adrenergic receptor agonist, UK-14,304, or the $G_{i/o}$ inhibitor, pertussis toxin (PTX, 200 or 750 ng/ml). Cells treated with PTX were pre-incubated with the toxin for 2 h prior to incubation with IBMX and subsequent stimulation with forskolin, as previously described [7,16]. Following forskolin stimulation, the cell suspension was quickly centrifuged at 4 °C, 3000 rpm for 10 min. Both the supernatant and pellet were quickly stored at −20 °C. cAMP levels were measured using a cAMP enzyme-linked immunosorbent assay by following the manufacturer's protocol (R&D Systems, Inc., Minneapolis, MN).

2.11. Data analysis and statistics

All values are presented as mean ± s.e.m. All statistical analyses were performed using GraphPad Prism 8.1.1 software for Mac OS X (Graph-Pad Software, San Diego, CA). Where appropriate, we used unpaired Student's *t*-test, repeated measures ANOVA (Analysis of variance), or mixed-effect model to determine significant interaction within and between groups. If the ANOVA or mixed-effect model yielded a significant effect of a factor or a significant interaction between multiple factors, Sidak post hoc analysis was used to determine significance of differences between groups, and results were considered significant if the *P* value was <0.05.

3. Results

3.1. Generation of Rgs2/5 dbKO mice

RGS2 and 5 are prominently expressed in cells of the cardiovascular and renal systems [24,25], and genetic ablation of either RGS protein is reported to cause hypertension in mice [13,26]. However, mice null for *Rgs2* or *Rgs5* have normal life span, and neither mouse model develops maladaptive cardiac hypertrophy or heart failure at baseline, despite exhibiting chronically elevated resting blood pressure [13,22]. These observations led us to hypothesize that the loss of RGS2 or 5 either triggers the activation of some yet unknown cardioprotective mechanism or increases the expression and/or function of other proteins that maintain the fine-tuning of G protein activity. To test these hypotheses, we sought to generate mice dually lacking RGS2 and 5. We crossed F1 double-heterozygous offspring resulting from single knockout ($Rgs2^{-/-}$ x $Rgs5^{-/-}$) crosses (Supplementary Fig. S1A). The

Rgs5$^{-/-}$ breeders were obtained from Dr. John Kehrl at the NIH-NIAID [15]. The *Rgs2*$^{-/-}$ mice, originally generated by Dr. Josef Penninger's group [14], were generously provided by Dr. Kendall Blumer at Washington University. All F2 offspring from the *Rgs2*$^{-/-}$ x *Rgs5*$^{-/-}$ crosses, including those that were null for *Rgs2* with one copy of *Rgs5*, those null for *Rgs5* with one copy of *Rgs2*, and those null for *Rgs2* and 5 (*Rgs2/5* dbKO) were viable without showing any developmental or gross abnormalities. All genotypes were confirmed by PCR using genomic DNA extracted from tail clips (Supplementary Fig. S1B). Contrary to a previous report regarding the gravimetric characteristics of *Rgs5*$^{-/-}$ mice [15], we did not find any difference in body weight. Similarly, the dual loss of RGS2 and 5 did not result in any difference in body weight (Supplementary Table S1).

3.2. Rgs2/5 dbKO mice develop spontaneous dilated cardiomyopathy

We examined the effects of the dual absence of RGS2 and 5 on baseline cardiac structure and function in male and female mice. We found, by gravimetric and echocardiographic assessments, that adult *Rgs2/5* dbKO mice developed unprovoked left ventricular dilatation, which was prominent in adult male mice (Fig. 1A-E). Although heart weight-to-tibia length ratio was higher in *Rgs2/5* dbKO mice, we found no difference in wet or dry cardiac tissue weight normalized to tibia length between the two genotypes (Supplementary Table S2). However, isolated cardiomyocytes from male *Rgs2/5* dbKO mice had a higher length-to-width ratio compared to cells from WT mice (Supplementary Table S3). The dilated left ventricle phenotype was age-dependent, since 30-day old pups had normal hearts, except for apparent ventricular hypertrophy in young female *Rgs2/5* dbKO mice (Fig. 1F & G). In adult male mice, heart rate measured from the anesthetized echocardiography data analysis was higher in WT relative to *Rgs2/5* dbKO mice (WT: 442 ± 19 bpm vs. *Rgs2/5* dbKO: 397 ± 12 bpm; $P = 0.03$). A similar trend was found in female mice; however, the difference did not reach statistical significance (WT: 432 ± 18 bpm vs. *Rgs2/5* dbKO: 390 ± 22 bpm; $P = 0.090$). Despite left ventricular dilatation, lung weight-to-body weight ratio of adult *Rgs2/5* dbKO mice was similar to that of WT control mice of the same sex (Fig. 1C), and no evidence of cardiac fibrosis was found (data not shown).

In addition to echocardiography, we used closed-chest pressure-volume (PV) loop approach to further assess cardiac structure and function in WT and *Rgs2/5 dbKO* mice under isoflurane anesthesia. Heart rate was similar between WT and *Rgs2/5* dbKO mice of both sexes (Fig. 2D). In male *Rgs2/5 dbKO* mice, percent ejection fraction (%EF) at baseline was low compared to WT cohort (Fig. 2 J), while stroke volume, cardiac output and slope of the end-systolic pressure-volume relationship (Ees) showed a decreasing trend (Fig. 2H, I, & K). Conversely, left ventricular systolic pressure, end-systolic volume (ESV) and arterial elastance (Ea) showed increasing trend in male *Rgs2/5 dbKO* mice (Fig. 2C, G & L). Interestingly, female *Rgs2/5* dbKO mice showed a marked elevation of Ees relative to WT mice of the same sex (Fig. 2K).

From a real-time PCR analysis, we did not find any marked changes in the expression of hallmark genes associated with maladaptive cardiac hypertrophy and fibrosis, including *Nppa, Myh7b, Tgfb1, Col3a1*, and *Ctgf*, except that female *Rgs2/5* dbKO hearts showed decreased expression of *Nppa* and *Ctgf* (Supplementary Fig. S2). In contrast, we found

significant changes in markers of cardiomyopathy. In female *Rgs2/5* dbKO hearts, there was a significant decrease in *Ttn, Tnnt2* and *Tnni3*, whereas male hearts showed a significant decrease in *Tnnt2* and a trend towards lower expression level of *Ttn* ($p = 0.1058$) and increasing trend in the expression of *Mybpc3* ($p = 0.0671$) (Supplementary Fig. S2, F-I). These findings are consistent with the hypothesis that the dual loss of RGS2 and 5 leads to a derangement in the homeostatic control of cardiac structure and function.

3.3. Hypo-responsiveness of Rgs2/5 dbKO hearts to acute β-adrenergic receptor stimulation

Because *Rgs2/5* dbKO mice showed reduced %EF and decreasing trend in %FS at baseline, we Tested whether the dual absence of RGS2 and 5 affected cardiac contractile reserve. To this end, we performed acute intraperitoneal infusion of the selective β_1AR agonist, dobutamine, while monitoring LV function by echocardiography under isoflurane anesthesia. As shown in Fig. 3, baseline percent fractional shortening (%FS) was low in male but not female *Rgs2/5 dbKO* mice compared to WT cohorts. Fig. 3 also shows that in male mice, dobutamine infusion caused a sharper increase in %FS, accompanied by a slightly steeper drop in heart rate relative to the response in *Rgs2/5* dbKO cohort. In female mice, %FS prior to dobutamine infusion was similar between genotypes. As seen in male mice, dobutamine infusion caused a sharper increase in %FS in female WT mice, however heart rate appeared to decline slightly faster in *Rgs2/5* dbKO relative to WT mice. These data indicated that myocardial responsiveness to βAR stimulation is impaired by the dual absence of RGS2 and 5, at least male mice.

3.4. Sex-dependent sudden death of Rgs2/5 dbKO mice following invasive surgery

Although gene expression analysis suggested the absence of maladaptive hypertrophy, we sought to examine baseline blood pressure to rule out ventricular hypertrophy resulting from potential pressure-overload. We assessed blood pressure by two approaches: using fluid-filled catheter under isoflurane anesthesia and in conscious, unrestrained condition by radiotelemetry approach involving a prior invasive surgery of telemeter implantation.

Baseline blood pressure under anesthesia was slightly elevated in male but not female *Rgs2/5* dbKO mice relative to WT cohorts (Fig. 4A). However, heart rate was similar between WT and *Rgs2/5* dbKO mice (Fig. 4B). As shown in Fig. 4C, we observed ~70% mortality only in male *Rgs2/5* dbKO mice during the recovery period following telemetry implantation surgery. To determine whether the high mortality rate in male *Rgs2/5* dbKO mice was preceded by extreme hypertension resulting from surgery-induced stress, we initiated blood pressure and heart rate monitoring immediately after radiotelemeter implantation surgery. As shown in Fig. 4D, male mice generally exhibited greater elevation of SBP within the first 24–48 h after surgery. Both diastolic blood pressure and heart rate were similar between the two genotypes. The initial stress-induced increase in SBP was more robust in *Rgs2/5* dbKO mice relative to wild type of the same sex. In male mice, diurnal blood pressure rhythm was re-established by day 4, but only SBP remained elevated in *Rgs2/5* dbKO mice by day 9 post surgery. In contrast, diurnal blood pressure rhythm in female mice was re-established within 72 h post-surgery, with the hypertensive phenotype becoming more evident after day 6 (Fig. 4E). These results indicated that acute

blood pressure elevation following surgery-induced stress was not sufficient to cause sex-dependent mortality of male *Rgs2/5* dbKO mice.

3.5. Acute in vivo β-adrenergic receptor stimulation induces both atrial and ventricular arrhythmias in Rgs2/5 dbKO male mice

To determine the cause of sudden death in male *Rgs2/5* dbKO mice a few days after telemetry surgery, we examined whether the dual absence of RGS2 and 5 increased the incidence of fatal cardiac events in response to sudden spikes in circulating catecholamines triggered by surgery-induced stress. We simulated sudden catecholamine surge by acute systemic administration of isoproterenol (ISO) to conscious mice instrumented with ECG telemetry implants for continuous monitoring of blood pressure and cardiac electrical activity. Prior to ISO administration, SBP was elevated in *Rgs2/5* dbKO male mice, whereas all baseline ECG parameters were similar between the two genotypes (Table 1).

Administration of ISO normalized blood pressure, reducing SBP by ~30 and ~ 50 mmHg in WT and *Rgs2/5* dbKO mice, respectively (Table 1). In addition to the effects on blood pressure, ISO administration reduced the height of T wave and increased ST interval in *Rgs2/5* dbKO mice. In both WT and *Rgs2/5* dbKO mice, the most prominent arrhythmic events observed at baseline included missed beats, ventricular ectopic (V Ectopic), single premature ventricular contractions (PVC Single), and sinus pause (Fig. 5A & 5B, blue tracings). Administration of ISO equally augmented the frequency of all the aforementioned arrhythmic events, except missed beats, which was reduced in *Rgs2/5* dbKO mice (Fig. 5A & 5B, orange tracings). To replicate whole-body stress as occurs after surgery, the mice were subjected to 90 min of involuntary swimming after which ECG was monitored for 30 min. Only P-R interval among the ECG parameters was markedly increased. However, as shown in Fig. 5C and D, stress from involuntary swimming increased the incidence of V Ectopic, PVC Single, and sinus pause relative to baseline, in WT mice. In contrast, sinus pause was the most prominent arrhythmic event in *Rgs2/5* dbKO mice following the swimming exercise (Fig. 5C & 5D, orange tracings). As happened after ISO administration, missed beats was markedly reduced after swimming. Together these results suggested that dual loss of RGS2 and 5 does not alter baseline arrhythmia burden but augments the occurrence of sinus pause due to stress.

3.6. Electrical field stimulation induces a sustained Ca^{2+} transient elevation and arrhythmias in ventricular myocytes from mice dually lacking Rgs2 and 5

To determine the underlying characteristics of the decreased myocardial contractility and arrhythmias resulting from the dual loss of RGS2 and 5 at the cellular level, we examined excitation-contraction coupling in vitro in freshly isolated adult left ventricular myocytes from male WT and *Rgs2/5 dbKO* mice. Application of electrical field stimulation (EFS) caused frequency-dependent increases in the speed of Ca^{2+} transients and contractility in cells from both genotypes (Fig. 6A). At the lowest EFS frequency (0.5 Hz), the maximal cardiomyocyte percent shortening (PS) was reduced in *Rgs2/5* dbKO cells, despite a higher Ca^{2+} transient amplitude (Fig. 6B-E). In WT cells, the application of EFS caused frequency-dependent decreases in PS and Ca^{2+} transients. In contrast, PS in *Rgs2/5* dbKO cardiomyocytes remained relatively unchanged, while Ca^{2+} transients continued to decrease

relative to baseline level (Fig. 6D & E). *Rgs2/5* dbKO cardiomyocytes showed prolonged contraction and cytoplasmic Ca^{2+} rise at 1–4 Hz, as determined by calculating the area under the curve of the respective signal traces from baseline to the peak for Ca^{2+} rise and contraction (Fig. 6F & G), and from the peak to baseline for relaxation and Ca^{2+} recycling (Fig. 6H & I).

In addition, we noted that the rate of shortening of *Rgs2/5* dbKO cardiomyocytes decreased relative to WT cells at higher EFS frequencies, particularly at 4 and 5 Hz (Fig. 6A-B, video #1 in supplementary data). The slowed contractile rate was interspersed with intermittent absence of Ca^{2+} transients and contractile response to the applied EFS (Fig 6A-B, arrows). Moreover, there were more *Rgs2/5* dbKO relative to WT cardiomyocytes (WT: 13% vs. *Rgs2/5 dbKO*: 63%) that developed sustained abnormal Ca^{2+} and contractile rhythms at 3–5 Hz (video #2 in supplementary data). Some cells, however, resumed normal contractile rhythm upon the return of EFS to baseline frequency of 0.5 Hz.

3.7. Dual loss of RGS2 and 5 augments the inhibitory activity of Gi/o, contributing to increased incidence of ventricular myocyte arrhythmias in response to EFS and βAR stimulation

RGS2 has been shown to negatively regulate β_2AR-$G_{i/o}$ signaling in the myocardium; accordingly, downregulation or the absence of RGS2 leads to decreased cardiomyocyte contractile response to βAR stimulation [7]. Because $G_{i/o}$ is also regulated by RGS5 [3], and that the loss of RGS5 also predisposes to arrhythmias [9,10], we reasoned that decreased contractility and increased rate of ventricular myocyte arrhythmias following the dual absence of RGS2 and 5 could be due, at least partly, to augmented inhibitory $G_{i/o}$ activity. To test this hypothesis, we compared $G_{i/o}$ activity in freshly isolated cardiomyocytes from WT, *Rgs2* KO, *Rgs5* KO and *Rgs2/5* dbKO male mice. In cellulo $G_{i/o}$ activity was assessed by measuring forskolin-stimulated cAMP generation in freshly isolated adult ventricular myocytes. As shown in Fig. 7, direct adenylyl cyclase activation with forskolin induced concentration-dependent increases in cAMP levels in WT cells, and these were attenuated by activating $G_{i/o}$ via the stimulation of the $G_{i/o}$-coupled α_2-adrenergic receptor with UK-14,304 (1 μM). Conversely, inhibiting $G_{i/o}$ by pre-incubation of the cells with pertussis toxin (PTX, 200 or 750 ng/ml) augmented forskolin-induced cAMP production in WT cells (Fig. 7). In *Rgs2* KO, *Rgs5* KO and *Rgs2/5* dbKO cardiomyocytes, forskolin-induced cAMP production was reduced. Of note, the suppression of cAMP generation in response to 50 μM forskolin appeared to be less pronounced in *Rgs5* KO cells relative to *Rgs2* KO and *Rgs2/5* dbKO cells. In addition, treatment with UK-14,304 had no effect on cAMP production in all three KO cell types. However, incubation of *Rgs2/5* dbKO cardiomyocytes with PTX augmented forskolin-induced cAMP production.

As was shown in Fig. 6, the application of EFS train triggered arrhythmias between 1 and 5 Hz in a fraction of cells from all genotypes, including cells from WT, *Rgs2* KO, *Rgs5* KO and *Rgs2/5* dbKO mice. Fig. 8 shows the quantification of arrhythmia incidence during EFS application, with most arrhythmias occurring at 5 Hz (Fig. 8A). The proportion of cells showing no arrhythmias during EFS application was similar between *Rgs2* KO, *Rgs5* KO,

and WT cells (*Rgs2* KO, ~80 vs. *Rgs5* KO, ~80 vs. WT, ~89%) but relatively lower in *Rgs2* dbKO cells (*Rgs2/5* dbKO, ~62% vs. WT, ~89%).

Fig. 8A also shows that inactivation of $G_{i/o}$ with 200 ng/ml PTX had little effect in WT cells but completely abolished arrhythmia incidence at all EFS frequencies in *Rgs2/5* dbKO cells. However, when a higher concentration (750 ng/ml) of PTX was applied, arrhythmias were detected at 5 Hz in WT cells and at 1, 3, and 5 Hz in *Rgs2/5* dbKO cells. By contrast, Fig. 8B shows that stimulation of cells with ISO induced arrhythmias at almost every concentration in all cells. Approximately 50% of WT cells developed no arrhythmias at all ISO concentrations. Notably, the percentage of *Rgs2/5* dbKO cells that never developed arrhythmia at any ISO concentration was about half the percentage in either *Rgs2* KO or *Rgs5* KO cells. Pretreatment with 200 or 750 ng/ml PTX increased ISO-induced arrhythmia development by ~10% in WT cells, whereas the same pretreatment decreased arrhythmia development by ~15% in *Rgs2/5* dbKO cells. These data together indicated that increased $G_{i/o}$ activity due to the dual absence of RGS2 and 5 is involved in receptor and non-receptor-dependent arrhythmia development in ventricular cardiomyocytes.

3.8. EFS-induced ventricular myocyte arrhythmias due to the dual absence of RGS2 and 5 are associated with exaggerated cytoplasmic Ca^{2+} elevation

Abnormal cytoplasmic Ca^{2+} handling has been implicated in ventricular myocyte arrhythmogenesis [27-31]. Because EFS-induced arrhythmias in cardiomyocytes from *Rgs2/5* dbKO male mice was accompanied by elevated cytoplasmic Ca^{2+}, we determined whether the dual absence of RGS2 and 5 affected the pathways involved in Ca^{2+} handling during excitation-contraction coupling. To determine whether altered Ca^{2+} extrusion pathways were involved in sustained elevation of cytoplasmic Ca^{2+}, we treated isolated ventricular myocytes with thapsigargin to block SERCA, followed by the application of EFS at 10 Hz (10 V) for 25 s, while monitoring cytoplasmic Ca^{2+} rise and decay. Fig. 9 shows that the application of EFS train induced an almost instantaneous rise in Ca^{2+} transients and myocyte shortening, both of which plateaued for the duration of the stimulation in both genotypes (Fig. 9A). The overall cytoplasmic Ca^{2+}rise, calculated as the area under the curve (AUC) of the fluorescence ratio-time curve for the duration of the EFS train, was elevated in *Rgs2/5* dbKO relative WT to cells. However, the AUC of the myocyte length-time curve for the same period was similar between the two groups, indicating similar levels of cardiomyocyte contraction (Fig. 9A & B). We then assessed the rate of cytoplasmic Ca^{2+} clearance by performing first order exponential decay curve fitting. The parameters in the equations shown in Fig. 9C indicate that although cytoplasmic Ca^{2+} at the end of the EFS train was significantly higher in *Rgs2/5* dbKO cells, the rate of Ca^{2+} removal from the cytoplasm, indicated by the time constant, was similar between the two groups. Using real-time PCR, we assessed myocardial mRNA levels of *Atp2a2* (SERCA2a), and *Slc8a1* (NCX_1) and *Atpb1* ($PMCA_1$), genes encoding proteins for Ca^{2+} reuptake into the SR and extrusion from the cardiomyocyte cytoplasm, respectively, to determine whether the augmented EFS-induced cytoplasmic Ca^{2+} rise was due at least partly to changes in gene expression. Supplementary Figs. S2 and S3 show that the dual absence of *Rgs2* and *5* did not affect the mRNA expression of SERCA2a, NCX_1, and $PMCA_1$ in freshly isolated cardiomyocytes. These results suggest that the exaggerated elevation of cytoplasmic Ca^{2+} in

Rgs2/5 dbKO cells is not due to decreased expression or altered activity of proteins involved in Ca^{2+} removal during *E*-C coupling events.

4. Discussion

The findings in this study reveal a novel understanding regarding the physiological relevance of the dual regulation of $G_{i/o}$ signaling by RGS2 and 5 in the heart. Besides having mildly elevated or reduced resting blood pressure, mice lacking RGS2 or RGS5 alone do not show any baseline cardiac phenotype except when subjected to experimental stressors including pressure overload and cardiac pacing [12,26,32,33]. Previous studies have also reported that the absence of RGS2 or 5 increases the incidence of atrial tachyarrhythmia induced with muscarinic receptor stimulation [34,35], and ventricular tachyarrhythmia in response to programmed electrical stimulation of isolated hearts [9,10]. Our findings now show that the dual absence of RGS2 and 5 causes unprovoked left ventricular dilatation without cardiomyocyte hypertrophy and independently of the associated baseline blood pressure elevation. In addition, the dual absence of RGS2 and 5 increases susceptibility to stress-induced cardiac arrhythmia and death that are mediated at least partly by aberrant signaling via β-adrenergic receptors and $G_{i/o}$ class G proteins. Moreover, our study suggests that RGS2 and 5 coordinate their regulatory activity towards $G_{i/o}$ signaling to facilitate normal ventricular myocyte rhythm.

Regulation of cardiac structure and function by the sympathetic nervous system is mediated by adrenergic receptors, including α- and β-adrenergic receptors (βAR) [36-38]. While α-adrenergic receptors couple mostly to $G_{q/11}$ and $G_{i/o}$ class G proteins for mobilization of Ca^{2+} from the SR, βAR on the other hand couple to both stimulatory G_s and inhibitory $G_{i/o}$ classes of heterotrimeric G proteins to regulate cAMP production [36,39]. $G_{q/11}$ signaling in many cell types, including cardiomyocytes, is fine-tuned by R4/B RGS proteins, most notably RGS2 and 5 [5,40,41]. Although specific RGS proteins that regulate G_s signaling are yet to be identified, there are emerging lines of evidence suggesting that RGS2 can regulate signaling downstream of this G protein class by interacting with adenylyl cyclase isoforms 5 and 6 in cells to negatively control cAMP production and affect cardiomyocyte contractile function [42-45]. Other lines of evidence also indicate that the inhibitory $G_{i/o}$ class G protein is regulated by many RGS proteins from other subfamilies beside R4/B RGS proteins in the heart [46,47]. However, evidence to date indicate that the regulation of $G_{i/o}$ by RGS2 and 5, individually, is critical to maintaining normal cardiac structure and function, since mice lacking RGS2 or 5 have been shown to be more sensitive to ISO-induced cardiac dysfunction and atrial fibrillation induced by cardiac pacing [6,7,9,10,35]. Despite these studies demonstrating the key roles of RGS2 and 5 in the myocardium, the fundamental questions that remain unexplored are how multiple RGS proteins coordinate their activity and, whether there is a functional redundancy in vivo in the fine-tuning of G protein signaling involved in the maintenance of normal physiology. Addressing these questions has been necessitated partly by previous studies showing that mice singly lacking RGS2 or 5 develop mild hypertension without any cardiac phenotype unless subjected to some experimental perturbation such as cardiac pacing or pressure-overload by transverse aortic constriction [12,22,35]. Because RGS2 and 5 both potently regulate $G_{q/11}$ and $G_{i/o}$, the dual absence of such key regulatory proteins was expected to be developmentally

detrimental. However, *Rgs2/5* dbKO mice are viable and appear normal and live to and beyond adulthood, suggesting that there is sufficient level of regulation by other proteins in the absence of potent regulators like RGS2 and 5 to ensure normal embryonic and postnatal development involving $G_{q/11}$ and $G_{i/o}$, signaling.

Here, we found that unlike the hearts of adult single *Rgs2* or *5* male KO mice [12,22], *Rgs2/5* dbKO mouse hearts are dilated at baseline. This cardiac phenotype is not accompanied by the hallmark maladaptive hypertrophy or increases in the expression of maladaptive hypertrophy markers such as *Nppa, Myh7b* and *Tgfb1*, nor is there increased lung weight-to-body weight ratio as seen in male $Rgs2^{-/-}$ or $Rgs5^{-/-}$ mice subjected to left ventricular pressure-overload [12,22]. Interestingly, we found cardiomyocytes from adult male *Rgs2/5* dbKO mice to be smaller in width but elongated relative to WT cells; however, there was no difference in cardiac weight between young and old mice (supplemental Table S1-3). These observations suggest that *Rgs2/5* dbKO cardiomyocytes increase in length to compensate for failure to undergo physiologic hypertrophy associated with myocardial maturation process to meet increasing circulatory demands in adulthood. Such developmental defects could trigger ventricular dilatation in an attempt to compensate for low cardiac mass for the maintenance of basal contractile function. However, such compensatory structural changes resulting from the dual absence of RGS2 and 5 appear insufficient for maintaining normal basal function, as indicated by lower basal ejection fraction and decreased contractile response to dobutamine-induced cardiac stress. Furthermore, adult *Rgs2/5* dbKO mice display elevated resting blood pressure and potential vascular stiffening indicated by elevated arterial elastance. These factors together increase left ventricular pressure-overload that usually triggers maladaptive cardiac hypertrophy, yet *Rgs2/5* dbKO hearts do not show any hypertrophy at baseline. We find this outcome surprising because pressure-overload induces maladaptive cardiac hypertrophy partly via augmented $G_{q/11}$ signaling, and both RGS2 and 5 have potent GAP activity towards this G protein class, and their overexpression in the heart has been shown to be cardioprotective, blocking pressure-overload hypertrophy [12,48-50]. Thus, the presence of LV dilatation-only cardiac phenotype at baseline suggests that pro-hypertrophic $G_{q/11}$ signaling is somehow still tightly regulated by other GAPs in the dual absence of RGS2 and 5. Instead, the dilated left ventricle in *Rgs2/5* dbKO mice, accompanied by changes in the expression of genes involved in Ca^{2+} sensing and cardiomyocyte contractility, and evident only in adult mice, is consistent with hypertrophic cardiomyopathy as opposed to pressure-overload hypertrophy and heart failure due to sustained hypertension [51]. Among the various forms of common cardiomyopathies known to date, the cardiac phenotype in *Rgs2/5* dbKO mice is most consistent with dilated cardiomyopathy [51] that is more noticeable in male mice. In addition, the expression of cardiomyopathy markers, particularly titin and troponin T, is reduced in *Rgs2/5* dbKO hearts of both sexes, and individual cardiomyocyte contractions are markedly decreased despite increased mobilization of intracellular Ca^{2+}. The augmented Ca^{2+} mobilization, however, appears to contribute to arrhythmogenesis as Ca^{2+} recycling is impaired, leading to prolonged elevation of cytoplasmic Ca^{2+} concentration, which is known to be arrhythmogenic [30,52-54]. Taken together with the decrease in the expression of contractile genes, our data suggest that the cardiomyopathy in *Rgs2/5* dbKO is accompanied by unraveling of the mechanisms that couple cardiac electrical excitation and contractility,

thereby contributing to the marked decrease in baseline ejection fraction and fractional shortening. These deficiencies may reduce cardiac reserve and increase susceptibility to an adverse cardiac event upon exertion from increased physical activity such as exercise or acute increases in cardiac catecholamine levels.

Indeed, this study shows that the dual inactivation of *Rgs2* and *5* greatly elevates the susceptibility to factors known to trigger cardiac events. As reported above, surgery-induced stress on the heart is sufficient to cause death in male *Rgs2/5* dBKO mice. Mechanistically, this is likely due to aberrant or unregulated βAR signaling resulting from sudden surges in cardiac sympathetic activation leading to exaggerated Ca^{2+} transients and prolonged elevation cytoplasmic Ca^{2+} level in ventricular myocytes. Consistent with this hypothesis, simulation of cardiac sympathetic overactivation and stress with acute administration of isoproterenol, or cardiomyocyte pacing, induced arrhythmia both in vivo and at single-cell levels, accompanied by substantial increases in cytoplasmic Ca^{2+}, while blockade of $G_{i/o}$ with pertussis toxin reduced arrhythmia incidents in *Rgs2/5* dbKO cardiomyocytes. Moreover, forskolin-induced cAMP generation was suppressed in *Rgs2/5* dbKO cardiomyocytes and was restored by inhibiting $G_{i/o}$ with pertussis toxin. These findings indicate that abnormal activity and the loss of regulation of βAR-$G_{i/o}$ signaling due to the dual absence of RGS2 and 5, at least partly, mediate cardiac arrhythmias in *Rgs2/5* dbKO ventricular cardiomyocytes. Although RGS2 is known to be a more potent GAP for $G_{q/11}$ and $G_{i/o}$, in vitro [55], expression at the mRNA level is substantially less than RGS5 in the cardiovascular system [56-58]. This suggests that the regulatory roles of RGS2 and 5 do not overlap. Here, we discovered that arrhythmia incidence resulting from EFS or βAR stimulation in *Rgs2/5* dbKO ventricular myocytes was roughly two times the level in either *Rgs2* KO or *Rgs5* KO myocytes. However, RGS2 appears to be more effective than RGS5 in finetuning $G_{i/o}$-dependent inhibition of adenylyl cyclase and thus cAMP generation in ventricular myocytes. Together, these findings suggest that RGS2 and 5 target different signaling pathways or different aspects of the same pathway that impinge on ventricular rhythm. In addition, the findings show that the relative strength of RGS2 and 5 as GAP towards $G_{i/o}$, in vivo may be different from previously established in vitro rank-order of GAP potencies B/R4 RGS proteins towards this inhibitory G protein class [55], as demonstrated in this study by the differences in the inhibition of forskolin-stimulated cAMP production upon $G_{i/o}$ activation with (α_2-adrenergic receptor stimulation.

Whereas the current study focused on the role of the dual loss of RGS2 and 5 in ventricular arrhythmias and βAR–$G_{i/o}$ signaling, previous reports by others have shown that mice null for *Rgs2* are more susceptible to tachypacing-induced atrial arrhythmia due, at least partly, to unregulated muscarinic M_3 receptor (M_3R) signaling [34,35]. Since M3R couples mainly to $G_{q/11}$ class G proteins, such reports suggest that the dysregulation of $G_{q/11}$ by RGS2 and/or 5 in the myocardium could contribute to ventricular arrhythmia. However, this possibility is likely not the case in *Rgs2/5* dbKO ventricular myocytes, since βAR, the primary mediator of cardiac sympathetic activity, do not couple to $G_{q/11}$ class G proteins. Thus, the findings here give novel insights into the mechanism by which $G_{i/o}$ signaling is dually regulated by RGS2 and 5 to facilitate normal cardiac rhythm. The discovery that the loss of RGS5 has minimal effects on forskolin-induced cAMP generation yet capable of compensating for RGS2 deficiency in mitigating ventricular myocyte arrhythmia should spur

additional studies to fully delineate how RGS2 and 5 regulate cellular responses dependent on $G_{i/o}$-adenylyl cyclase-cAMP signaling.

Other notable observations in this study are the sex-related differences in the cardiac structural and functional changes resulting from the dual loss of RGS2 and 5. Although female *Rgs2/5* dbKO mice displayed apparent cardiac hypertrophy, this was not accompanied by LV dilatation as in male mice or death following surgery-related stress. In addition, there was no effect of the dual absence of RGS2 and 5 on the response to cardiac stress test with acute dobutamine infusion. The lack of difference in the dobutamine stress test in female mice could be due to compensation by other RGS proteins. However, this possibility was ruled out as gene expression analysis showed no compensatory increase in the mRNA expression of other members of the B/R4 RGS family expressed in the cardiovascular system (Supplementary Fig. S4). Interestingly, we noted that in both sexes of *Rgs2/5* dbKO mice, there was a substantial decrease in the mRNA expression of RGS4, which is prominently expressed in the myocardium and also acts a potent GAP towards $G_{i/o}$ class G proteins [24,58,59]. We also noted that changes in gene markers of cardiomyopathy was more prominent in the hearts of female *Rgs2/5* dbKO mice, suggesting potential sex differences in the pathogenesis of cardiomyopathy resulting from the dual absence of RGS2 and 5. The mechanisms mediating sex-related differences in the cardiac phenotype resulting from the dual absence of RGS2 and 5 was not explored in this study. However, it is noteworthy that numerous studies have established the cardioprotective role of ovarian hormones [60-62]. For instance, ovariectomized female rats subjected to chronic volume overload displayed eccentric cardiac hypertrophy accompanied by LV dilatation, which were reversed by exogenous estrogen treatment [62]. These previous observations warrant further studies to assess the potential interplay between RGS function and the protective role of sex hormones in the heart.

In summary, this study demonstrates the critical role of the coordinated relationship between RGS2 and 5 in regulating signaling via $G_{i/o}$ class G proteins to facilitate normal cardiac structure and function. A deeper probing of the coordination between the expression and function of RGS2 and 5 in other cells and organ systems is necessary to enhance the understanding of regulatory balance of RGS proteins for promoting homeostasis.

Supplementary Material

Refer to Web version on PubMed Central for supplementary material.

Acknowledgements

We thank Professor Kendall J. Blumer at Washington University School of Medicine in St. Louis, MO and Dr. John Kehrl at the NIH-NIAID for generously providing the *Rgs2*$^{-/-}$ and *Rgs5*$^{-/-}$ mice, respectively. We also thank all members of the Osei-Owusu lab for technical assistance and for comments on the manuscript.

Funding

The study was supported in part by grants from the American Heart Association (16SDG27260276), and the National Institutes of Health (R01 HL139754) to Patrick Osei-Owusu. The funding agencies had no role in the study design or execution.

References

[1]. Cadrin-Tourigny J, Shohoudi A, Roy D, Talajic M, Tadros R, Mondesert B, Dyrda K, Rivard L, Andrade JG, Macle L, Guerra PG, Thibault B, Dubuc M, Khairy P, Decreased mortality with beta-blockers in patients with heart failure and coexisting atrial fibrillation: an AF-CHF substudy, JACC Heart Fail. 5 (2017) 99–106. [PubMed: 28089316]

[2]. Hepler JR, Gilman AG, proteins G, Trends Biochem. Sci. 17 (1992) 383–387.

[3]. Chidiac P, Roy AA, Activity, regulation, and intracellular localization of RGS proteins, Recept. Channels 9 (2003) 135–147. [PubMed: 12775336]

[4]. Riddle EL, Schwartzman RA, Bond M, Insel PA, Multi-tasking RGS proteins in the heart: the next therapeutic target? Circ. Res 96 (2005) 401–411. [PubMed: 15746448]

[5]. Osei-Owusu P, Blumer KJ, Regulator of G protein signaling 2: a versatile regulator of vascular function, Prog. Mol. Biol. Transl. Sci 133 (2015) 77–92. [PubMed: 26123303]

[6]. Hao J, Michalek C, Zhang W, Zhu M, Xu X, Mende U, Regulation of cardiomyocyte signaling by RGS proteins: differential selectivity towards G proteins and susceptibility to regulation, J. Mol. Cell. Cardiol 41 (2006) 51–61. [PubMed: 16756988]

[7]. Chakir K, Zhu W, Tsang S, Woo AY, Yang D, Wang X, Zeng X, Rhee MH, Mende U, Koitabashi N, Takimoto E, Blumer KJ, Lakatta EG, Kass DA, Xiao RP, RGS2 is a primary terminator of beta(2)-adrenergic receptor-mediated G(i) signaling, J. Mol. Cell. Cardiol 50 (2011) 1000–1007. [PubMed: 21291891]

[8]. Zhang P, Mende U, Functional role, mechanisms of regulation, and therapeutic potential of regulator of G protein signaling 2 in the heart, Trends Cardiovasc. Med 24 (2014) 85–93. [PubMed: 23962825]

[9]. Qin M, Huang H, Wang T, Hu H, Liu Y, Cao H, Li H, Huang C, Absence of Rgs5 prolongs cardiac repolarization and predisposes to ventricular tachyarrhythmia in mice, J. Mol. Cell. Cardiol 53 (2012) 880–890. [PubMed: 23079193]

[10]. Qin M, Liu X, Liu T, Wang T, Huang C, Potential role of regulator of G-protein signaling 5 in the protection of vagal-related bradycardia and atrial tachyarrhythmia, J. Am. Heart Assoc 5 (2016), e002783. [PubMed: 26961238]

[11]. Anger T, Klintworth N, Stumpf C, Daniel WG, Mende U, Garlichs CD, RGS protein specificity towards Gq- and Gi/o-mediated ERK 1/2 and Akt activation, in vitro, J. Biochem. Mol. Biol 40 (2007) 899–910. [PubMed: 18047785]

[12]. Li H, He C, Feng J, Zhang Y, Tang Q, Bian Z, Bai X, Zhou H, Jiang H, Heximer SP, Qin M, Huang H, Liu PP, Huang C, Regulator of G protein signaling 5 protects against cardiac hypertrophy and fibrosis during biomechanical stress of pressure overload, Proc. Natl. Acad. Sci. U. S. A 107 (2010) 13818–13823. [PubMed: 20643937]

[13]. Holobotovskyy V, Manzur M, Tare M, Burchell J, Bolitho E, Viola H, Hool LC, Arnolda F, McKitrick DJ, Ganss R, Regulator of G-protein signaling 5 controls blood pressure homeostasis and vessel wall remodeling, Circ. Res 112 (2013) 781–791. [PubMed: 23303165]

[14]. Oliveira-Dos-Santos AJ, Matsumoto G, Snow BE, Bai D, Houston FP, Whishaw IQ, Mariathasan S, Sasaki T, Wakeham A, Ohashi PS, Roder JC, Barnes CA, Siderovski DP, Penninger JM, Regulation of T cell activation, anxiety, and male aggression by RGS2, Proc. Natl. Acad. Sci. U. S. A 97 (2000) 12272–12277. [PubMed: 11027316]

[15]. Cho H, Park C, Hwang IY, Han SB, Schimel D, Despres D, Kehrl JH, Rgs5 targeting leads to chronic low blood pressure and a lean body habitus, Mol. Cell. Biol 28 (2008) 2590–2597. [PubMed: 18268011]

[16]. Osei-Owusu P, Sabharwal R, Kaltenbronn KM, Rhee MH, Chapleau MW, Dietrich HH, Blumer KJ, Regulator of G protein signaling 2 deficiency causes endothelial dysfunction and impaired endothelium-derived hyperpolarizing factor-mediated relaxation by dysregulating Gi/o signaling, J. Biol. Chem 287 (2012) 12541–12549. [PubMed: 22354966]

[17]. Osei-Owusu P, Owens EA, Jie L, Reis JS, Forrester SJ, Kawai T, Eguchi S, Singh H, Blumer KJ, Regulation of renal hemodynamics and function by RGS2, PLoS One 10 (2015), e0132594. [PubMed: 26193676]

[18]. Owens EA, Jie L, Reyes BAS, Van Bockstaele EJ, Osei-Owusu P, Elastin insufficiency causes hypertension, structural defects and abnormal remodeling of renal vascular signaling, Kidney Int. 92 (2017) 1100–1118. [PubMed: 28754555]

[19]. Rogers JH, Tamirisa P, Kovacs A, Weinheimer C, Courtois M, Blumer KJ, Kelly DP, Muslin AJ, RGS4 causes increased mortality and reduced cardiac hypertrophy in response to pressure overload, J. Clin. Invest 104 (1999) 567–576. [PubMed: 10487771]

[20]. Puhl SL, Weeks KL, Ranieri A, Avkiran M, Assessing structural and functional responses of murine hearts to acute and sustained beta-adrenergic stimulation in vivo, J. Pharmacol. Toxicol. Methods 79 (2016) 60–71. [PubMed: 26836145]

[21]. Gao S, Ho D, Vatner DE, Vatner SF, Echocardiography in mice, Curr. Protoc. Mouse Biol 1 (2011) 71–83. [PubMed: 21743841]

[22]. Takimoto E, Koitabashi N, Hsu S, Ketner EA, Zhang M, Nagayama T, Bedja D, Gabrielson KL, Blanton R, Siderovski DP, Mendelsohn ME, Kass DA, Regulator of G protein signaling 2 mediates cardiac compensation to pressure overload and antihypertrophic effects of PDE5 inhibition in mice, J. Clin. Invest 119 (2009) 408–420. [PubMed: 19127022]

[23]. Ackers-Johnson M, Li PY, Holmes AP, O'Brien SM, Pavlovic D, Foo RS, A simplified, Langendorff-free method for concomitant isolation of viable cardiac myocytes and nonmyocytes from the adult mouse heart, Circ. Res 119 (2016) 909–920. [PubMed: 27502479]

[24]. Gu S, Cifelli C, Wang S, Heximer SP, RGS proteins: identifying new GAPs in the understanding of blood pressure regulation and cardiovascular function, Clin. Sci 116 (2009) 391–399.

[25]. Ganss R, Keeping the balance right: regulator of G protein signaling 5 in vascular physiology and pathology, Prog. Mol. Biol. Transl. Sci 133 (2015) 93–121. [PubMed: 26123304]

[26]. Heximer SP, Knutsen RH, Sun X, Kaltenbronn KM, Rhee MH, Peng N, Oliveira-dos-Santos A, Penninger JM, Muslin AJ, Steinberg TH, Wyss JM, Mecham RP, Blumer KJ, Hypertension and prolonged vasoconstrictor signaling in RGS2-deficient mice, J. Clin. Invest 111 (2003) 445–452. [PubMed: 12588882]

[27]. Nemec J, Kim JJ, Salama G, The link between abnormal calcium handling and electrical instability in acquired long QT syndrome – does calcium precipitate arrhythmic storms? Prog. Biophys. Mol. Biol 120 (2016) 210–221. [PubMed: 26631594]

[28]. Pogwizd SM, Bers DM, Cellular basis of triggered arrhythmias in heart failure, Trends Cardiovasc. Med 14 (2004) 61–66. [PubMed: 15030791]

[29]. Chelu MG, Wehrens XH, Sarcoplasmic reticulum calcium leak and cardiac arrhythmias, Biochem. Soc. Trans 35 (2007) 952–956. [PubMed: 17956253]

[30]. Landstrom AP, Dobrev D, Wehrens XHT, Calcium signaling and cardiac arrhythmias, Circ. Res 120 (2017) 1969–1993. [PubMed: 28596175]

[31]. Tamayo M, Fulgencio-Covian A, Navarro-Garcia JA, Val-Blasco A, Ruiz-Hurtado G, Gil-Fernandez M, Martin-Nunes L, Lopez JA, Desviat LR, Delgado C, Richard E, Fernandez-Velasco M, Intracellular calcium mishandling leads to cardiac dysfunction and ventricular arrhythmias in a mouse model of propionic acidemia, Biochim. Biophys. Acta Mol. basis Dis 1866 (2020), 165586. [PubMed: 31678161]

[32]. Arnold C, Demirel E, Feldner A, Genove G, Zhang H, Sticht C, Wieland T, Hecker M, Heximer S, Korff T, Hypertension-evoked RhoA activity in vascular smooth muscle cells requires RGS5, FASEB J. 32 (2018) 2021–2035. [PubMed: 29208700]

[33]. Tang KM, Wang GR, Lu P, Karas RH, Aronovitz M, Heximer SP, Kaltenbronn KM, Blumer KJ, Siderovski DP, Zhu Y, Mendelsohn ME, Regulator of G-protein signaling-2 mediates vascular smooth muscle relaxation and blood pressure, Nat. Med 9 (2003) 1506–1512. [PubMed: 14608379]

[34]. Jones DL, Tuomi JM, Chidiac P, Role of cholinergic innervation and RGS2 in atrial arrhythmia, Front. Physiol 3 (2012) 239. [PubMed: 22754542]

[35]. Tuomi JM, Chidiac P, Jones DL, Evidence for enhanced M3 muscarinic receptor function and sensitivity to atrial arrhythmia in the RGS2-deficient mouse, Am. J. Physiol. Heart Circ. Physiol 298 (2010) H554–H561. [PubMed: 19966055]

[36]. Xiao RP, Beta-adrenergic signaling in the heart: dual coupling of the beta2-adrenergic receptor to G(s) and G(i) proteins, Sci. STKE 2001 (2001), re15. [PubMed: 11604549]

[37]. Xiao RP, Cheng H, Zhou YY, Kuschel M, Lakatta EG, Recent advances in cardiac beta(2)-adrenergic signal transduction, Circ. Res 85 (1999) 1092–1100. [PubMed: 10571541]

[38]. Schmitz W, Eschenhagen T, Mende U, Muller FU, Scholz H, The role of alpha 1-adrenergic and muscarinic receptors in cardiac function, Eur. Heart J 12 (Suppl F) (1991) 83–87.

[39]. Esler M, Kaye D, Lambert G, Esler D, Jennings G, Adrenergic nervous system in heart failure, Am. J. Cardiol 80 (1997) 7L–14L.

[40]. Anger T, Zhang W, Mende U, Differential contribution of GTPase activation and effector antagonism to the inhibitory effect of RGS proteins on Gq-mediated signaling in vivo, J. Biol. Chem 279 (2004) 3906–3915. [PubMed: 14630933]

[41]. Bansal G, Druey KM, Xie Z, R4 RGS proteins: regulation of G-protein signaling and beyond, Pharmacol. Ther 116 (2007) 473–495. [PubMed: 18006065]

[42]. Roy AA, Baragli A, Bernstein LS, Hepler JR, Hebert TE, Chidiac P, RGS2 interacts with Gs and adenylyl cyclase in living cells, Cell. Signal 18 (2006) 336–348. [PubMed: 16095880]

[43]. Sjogren B, Parra S, Atkins KB, Karaj B, Neubig RR, Digoxin-mediated upregulation of RGS2 protein protects against cardiac injury. J. Pharmacol. Exp. Ther 357 (2016) 311–319. [PubMed: 26941169]

[44]. Salim S, Dessauer CW, Analysis of the interaction between RGS2 and adenylyl cyclase, Methods Enzymol. 390 (2004) 83–99. [PubMed: 15488172]

[45]. Salim S, Sinnarajah S, Kehrl JH, Dessauer CW, Identification of RGS2 and type V adenylyl cyclase interaction sites, J. Biol. Chem 278 (2003) 15842–15849. [PubMed: 12604604]

[46]. Yang J, Huang J, Maity B, Gao Z, Lorca RA, Gudmundsson H, Li J, Stewart A, Swaminathan PD, Ibeawuchi SR, Shepherd A, Chen CK, Kutschke W, Mohler PJ, Mohapatra DP, Anderson ME, Fisher RA, RGS6, a modulator of parasympathetic activation in heart, Circ. Res 107 (2010) 1345–1349. [PubMed: 20864673]

[47]. Parra S, Huang X, Charbeneau RA, Wade SM, Kaur K, Rorabaugh BR, Neubig RR, Conditional disruption of interactions between Galphai2 and regulator of G protein signaling (RGS) proteins protects the heart from ischemic injury, BMC Pharmacol. Toxicol 15 (2014) 29. [PubMed: 24899231]

[48]. Lee KN, Lu X, Nguyen C, Feng Q, Chidiac P, Cardiomyocyte specific overexpression of a 37 amino acid domain of regulator of G protein signalling 2 inhibits cardiac hypertrophy and improves function in response to pressure overload in mice, J. Mol. Cell. Cardiol 108 (2017) 194–202. [PubMed: 28641980]

[49]. Park-Windhol C, Zhang P, Zhu M, Su J, Chaves L Jr., Maldonado AE, King ME, Rickey L, Cullen D, Mende U, Gq/11-mediated signaling and hypertrophy in mice with cardiac-specific transgenic expression of regulator of G-protein signaling 2, PLoS One 7 (2012), e40048. [PubMed: 22802950]

[50]. Nunn C, Zou MX, Sobiesiak AJ, Roy AA, Kirshenbaum LA, Chidiac P, RGS2 inhibits beta-adrenergic receptor-induced cardiomyocyte hypertrophy, Cell. Signal 22 (2010) 1231–1239. [PubMed: 20362664]

[51]. Marsiglia JD, Pereira AC, Hypertrophic cardiomyopathy: how do mutations lead to disease? Arq. Bras. Cardiol 102 (2014) 295–304. [PubMed: 24714796]

[52]. Lin DJ, Lee WS, Chien YC, Chen TY, Yang KT, The link between abnormalities of calcium handling proteins and catecholaminergic polymorphic ventricular tachycardia, Tzu Chi Med. J 33 (2021) 323–331. [PubMed: 34760626]

[53]. Lotteau S, Zhang R, Hazan A, Grabar C, Gonzalez D, Aynaszyan S, Philipson KD, Ottolia M, Goldhaber JI, Acute genetic ablation of cardiac sodium/calcium exchange in adult mice: implications for cardiomyocyte calcium regulation, cardioprotection, and arrhythmia, J. Am. Heart Assoc 10 (2021), e019273. [PubMed: 34472363]

[54]. Kistamas K, Veress R, Horvath B, Banyasz T, Nanasi PP, Eisner DA, Calcium handling defects and cardiac arrhythmia syndromes, Front. Pharmacol 11 (2020) 72. [PubMed: 32161540]

[55]. Watson N, Linder ME, Druey KM, Kehrl JH, Blumer KJ, RGS family members: GTPase-activating proteins for heterotrimeric G-protein alpha-subunits, Nature 383 (1996) 172–175. [PubMed: 8774882]

[56]. Jiang H, Xie Y, Abel PW, Wolff DW, Toews ML, Panettieri RA Jr., Casale TB, Tu Y, RGS2 repression exacerbates airway hyperresponsiveness and remodeling in asthma, Am. J. Respir. Cell Mol. Biol 53 (1) (2014) 42–49, 10.1165/rcmb.2014-0319OC.

[57]. Koch JN, Dahlen SA, Owens EA, Osei-Owusu P, Regulator of G protein signaling 2 facilitates uterine artery adaptation during pregnancy in mice, J. Am. Heart Assoc 8 (2019), e010917. [PubMed: 31030617]

[58]. Mittmann C, Chung CH, Hoppner G, Michalek C, Nose M, Schuler C, Schuh A, Eschenhagen T, Weil J, Pieske B, Hirt S, Wieland T, Expression of ten RGS proteins in human myocardium: functional characterization of an upregulation of RGS4 in heart failure, Cardiovasc. Res 55 (2002) 778–786. [PubMed: 12176127]

[59]. Jaba IM, Zhuang ZW, Li N, Jiang Y, Martin KA, Sinusas AJ, Papademetris X, Simons M, Sessa WC, Young LH, Tirziu D, NO triggers RGS4 degradation to coordinate angiogenesis and cardiomyocyte growth, J. Clin. Invest 123 (2013) 1718–1731. [PubMed: 23454748]

[60]. Brower GL, Gardner JD, Janicki JS, Gender mediated cardiac protection from adverse ventricular remodeling is abolished by ovariectomy, Mol. Cell. Biochem 251 (2003) 89–95. [PubMed: 14575309]

[61]. Rosano GM, Chierchia SL, Leonardo F, Beale CM, Collins P, Cardioprotective effects of ovarian hormones, Eur. Heart J 17 (Suppl D) (1996) 15–19. [PubMed: 8869877]

[62]. Gardner JD, Brower GL, Voloshenyuk TG, Janicki JS, Cardioprotection in female rats subjected to chronic volume overload: synergistic interaction of estrogen and phytoestrogens, Am. J. Physiol. Heart Circ. Physiol 294 (2008) H198–H204. [PubMed: 17965290]

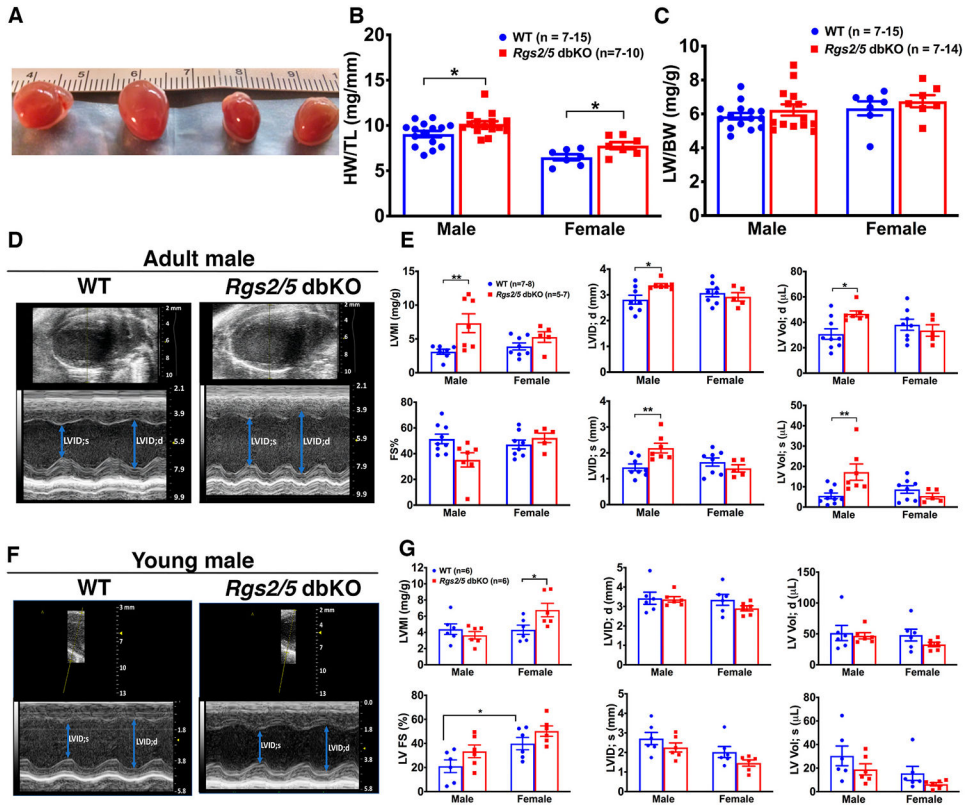

Fig. 1.

Cardiac phenotype of *Rgs2/5* dbKO mice. A) Representative images of apparent cardiac hypertrophy in adult male and female *Rgs2/5* dbKO mice compared to their WT cohorts. B) Gravimetric analysis showing increased heart weight in female ($n = 7$ of each genotype) and male ($n = 10$ of each genotype) WT vs. *Rgs2/5* dbKO mice. Heart weight (HW) was normalized to tibia length (TL). C) Lung weight (LW) of WT and *Rgs2/5* dbKO female and male mice was normalized to body weight (BW). D) Representative B- (top) and M-mode (bottom) of left ventricular (LV) echocardiographs of adult male WT and *Rgs2/5* dbKO mice acquired under isoflurane anesthesia. E) Summarized results of analyzed echocardiographs of adult WT and *Rgs2/5* dbKO mice ($n = 5$ of each genotype and sex). F) Representative B- (top) and M-mode (bottom) of left ventricular (LV) echocardiographs of young (30 days old) male WT and *Rgs2/5* dbKO mice acquired under isoflurane anesthesia. G) Summarized results of analyzed echocardiographs of young WT and *Rgs2/5* dbKO mice ($n = 6$ of each genotype and sex). Bar graph values are mean ± s.e.m. LV internal dimension at systole (LVID;s) and at diastole (LVID;d) are indicated by the bidirectional arrows in the echocardiograms. LVMI, LV mass index; LV Vol;d, LV volume at diastole; LV Vol;s, LV volume at systole; LV FS, LV fractional shortening. *, **$P < 0.05, 0.01$.

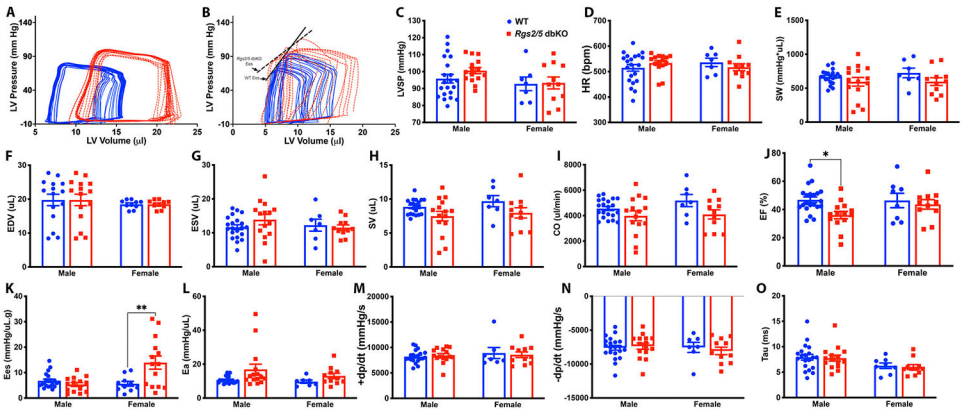

Fig. 2.

Examination of baseline cardiac function using pressure-volume (PV) loop analysis of left ventricle hemodynamics. A, B) Representative PV loops at baseline and during occlusion of the inferior vena cava in male wild type (solid blue lines) and *Rgs2* dbKO (dash red lines) mice. Steepness of the end-systolic pressure volume relationship (Ees), reflecting contractile function of each genotype, is indicated by the black tangent lines. C – O) Bar graphs showing summary data from analysis of 10–15 PV loops of male and female WT (n = 20 male & 8 female) and *Rgs2/5* dbKO (n = 15 male & 11 female) mice. Male *Rgs2/5* dbKO hearts display reduced ejection fraction (EF), with trends towards decreased stroke volume (SV) and cardiac output, and enlarged left ventricle, while female *Rgs2/5* dbKO hearts show augmented end-systolic elastance (Ees), reflecting increased contractile function. Both male and female *Rgs2/5* dbKO mice show a trend towards increased arterial elastance (Ea), reflecting increased total ventricular afterload likely resulting from elevated systolic blood pressure. Bar graph values are mean ± s.e.m. LVSP, left ventricular systolic pressure; CO, cardiac output; ESV, end-systolic volume; EDV, end-diastolic volume; Tau, relaxation time constant; +dp/dt, peak rate of LV pressure rise; −dp/dt, peak rate of LV pressure decline; SW, stroke work. P values were obtained by 2-way ANOVA for sex and genotype, followed by Sidak post hoc test.

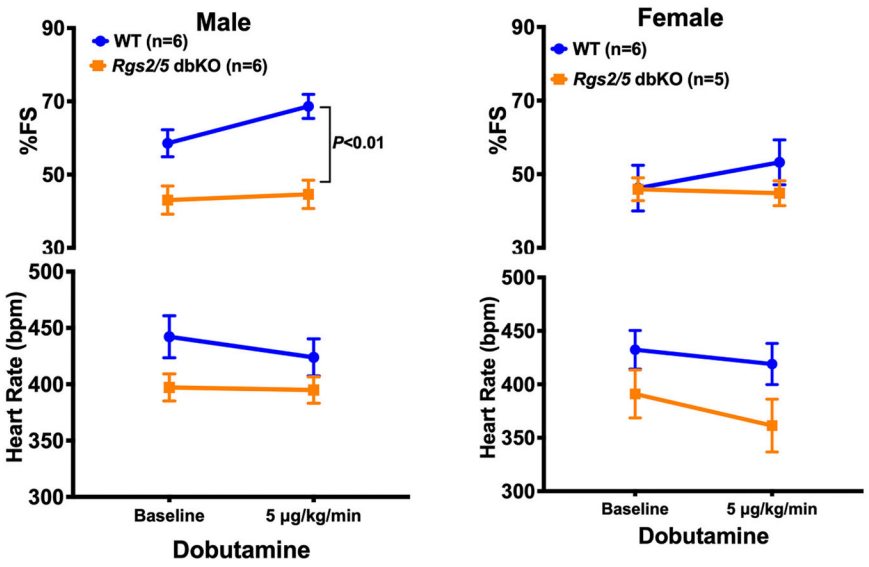

Fig. 3.

Echocardiographic analysis of changes in percent fractional shortening (%FS) and heart rate of male and Female WT (n = 6 male & 6 female) and *Rgs2/5* dbKO (n = 6 male & 5 female) mice in response to acute intraperitoneal infusion of the β1-adrenergic agonist, dobutamine, under isoflurane anesthesia. A working solution of dobutamine hydrochloride (Dobutamine, 10 μg/μl) was prepared from dobutamine stock (1 g/ml in DMSO) in 1:100 dilution in normal saline. After baseline acquisition, each mouse received intraperitoneal infusion of dobutamine (5 μg/kg/min) for 1 min, using an infusion pump. Changes in left ventricular M-mode fractional shortening in response to the infusion were calculated offline. Values are mean ± s.e.m. P value was repeated measures ANOVA followed by Sidak post hoc test.

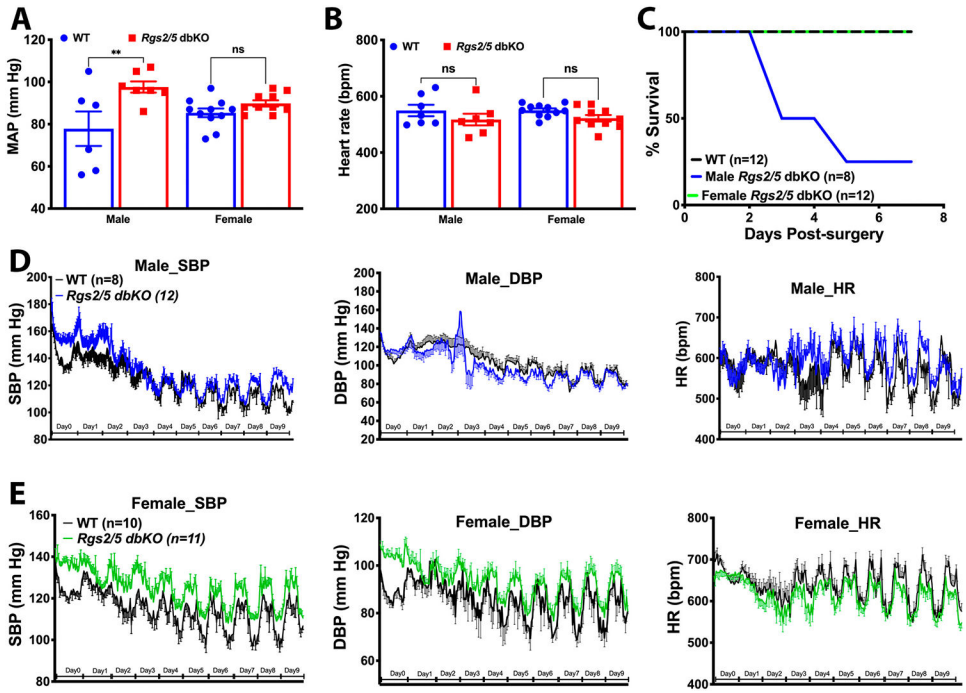

Fig. 4.

Baseline blood pressure and heart rate of male and female WT and *Rgs2* dbKO mice measured under isoflurane anesthesia and in conscious state. A, B) Mean arterial pressure (MAP) and heart rate, respectively, of WT and *Rgs2/5* dbKO mice under isoflurane anesthesia. C) Survival curve of WT and *Rgs2/5* dbKO mice following telemetry implantation surgery. Systolic blood pressure, diastolic blood pressure (DBP), and heart rate (HR) of male (D) and female (E) mice were monitored starting immediately after the surgical procedure and throughout the recovery period. Values are mean ± s.e.m. $^{**}P < 0.05$, 0.01.

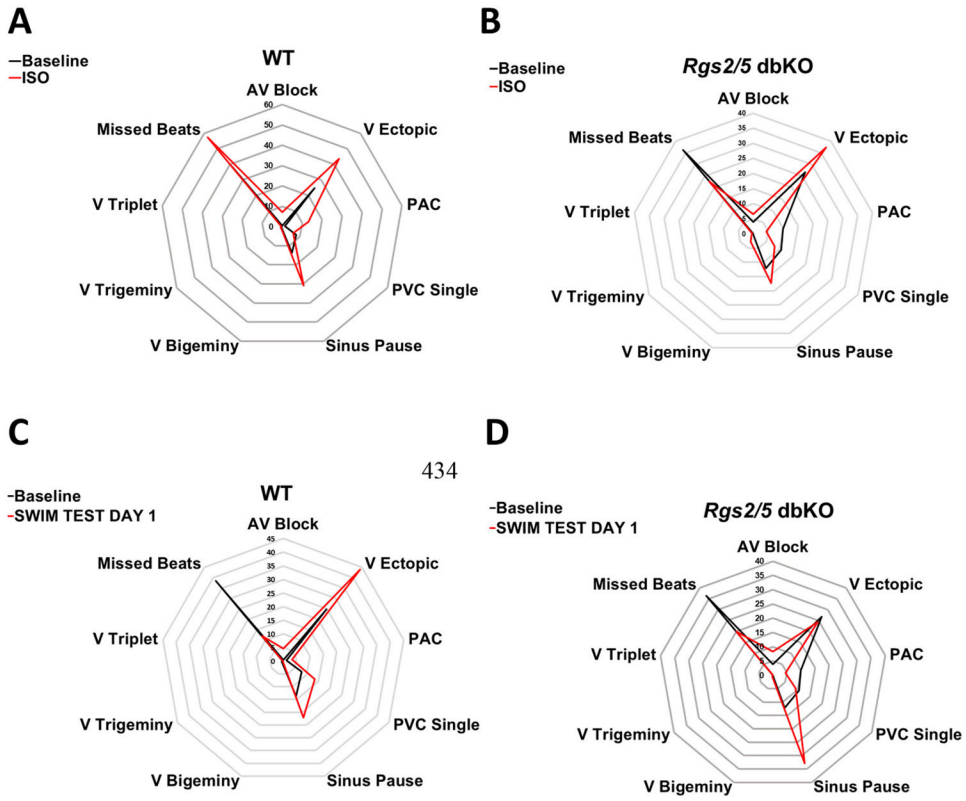

434

Fig. 5.

Summary data of telemetry electrocardiography (ECG) from conscious male WT and *Rgs2/5* dbKO mice before and after acute intraperitoneal administration of the non-selective β-adrenergic agonist, isoproterenol (ISO) and during involuntary swimming. A) Web graphs of male WT ($n = 4$) and *Rgs2/5* dbKO ($n = 5$) mice before and after a bolus ISO injection (0.75 mg/kg, i.p.). B) Web graphs of male WT (n = 4) and *Rgs2/5* dbKO (n = 5) mice before and during a 90-min forced-swim exercise. The frequency of each cardiac event at baseline was calculated as percent of total events in each genotype, while the frequency after ISO injection was calculated as percent change of a given event from baseline of the genotype. AV block, atrio-ventricular block; V ectopic, ventricular ectopic; PAC, premature atrial contraction; PVC Single, single premature ventricular contraction; V Bigeminy, ventricular bigeminy; V Trigeminy, ventricular trigeminy; V triplet, ventricular triplet.

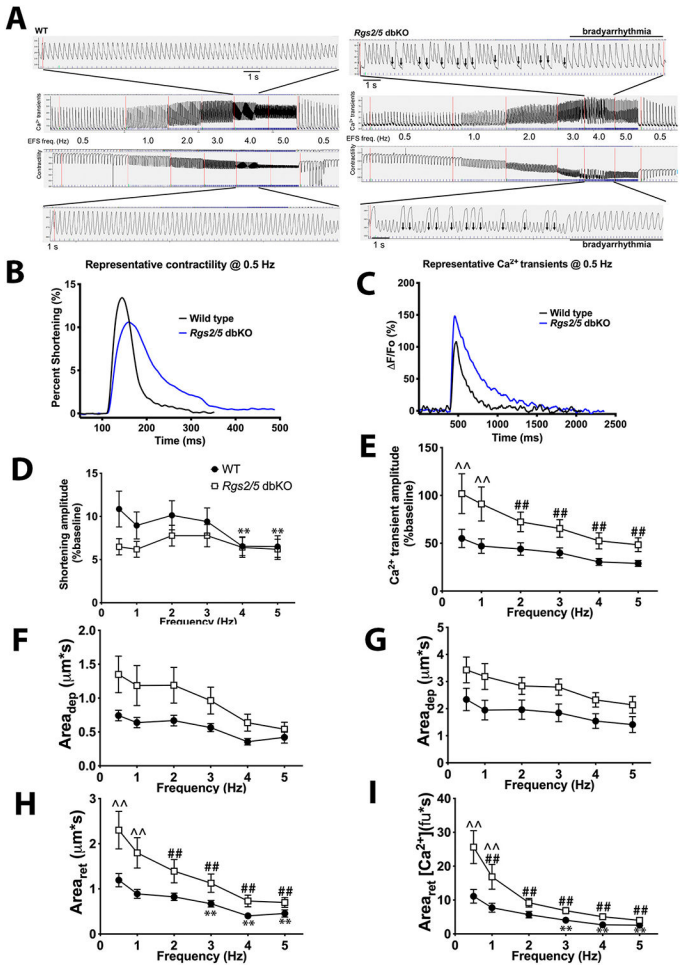

Fig. 6.

Adult left ventricular myocytes from male *Rgs2/5* dbKO mice show impaired excitation-contraction (*E*-C) coupling. A) Representative tracings of Ca^{2+} transients and contractility, respectively, of male WT and *Rgs2/5* dbKO cardiomyocytes subjected to a train of electrical field stimulation (EFS, 10 V at 0.5–5.0 Hz). The zoom-in of the E-C coupling tracings show a slower rate of contraction and missing Ca^{2+} transients and contractions (arrows) in tracings from *Rgs2/5* dbKO cardiomyocytes. B, C) Representative tracings of single contractility (left) and Ca^{2+} transients (right) of male WT and *Rgs2/5* dbKO cardiomyocytes subjected to EFS at 0.5 Hz. D – I) Summary graphs of contractility and calcium transient characteristics during EFS application in cardiomyocytes from male WT and *Rgs2/5* dbKO mice (n = 50 cells from 9 to 12 hearts of each genotype). Cardiomyocytes from *Rgs2/5* dbKO mice show increased amplitude of Ca^{2+} transients without a corresponding increase in percent shortening or contractility relative to the response in WT cells (D & E). Both the overall level of contraction and the amount of cytosolic Ca^{2+} accumulation, determined by the area under the curve from the start to the peak of the contractile and transient traces (F & G), are augmented in *Rgs2* dbKO cells. Similarly, relaxation and clearance of cytosolic Ca^{2+} (H & I) are delayed in *Rgs2* dbKO relative to WT cells. All values are mean ± s.e.m. $^{**}P < 0.01$ vs. WT at 0.5 Hz; $^{\#\#}P < 0.01$ vs. *Rgs2* dbKO at 0.5 Hz; $\wedge\wedge P < 0.01$ WT vs. *Rgs2* dbKO. *P* values were from Sidak post hoc analysis following a mixed-effects ANOVA.

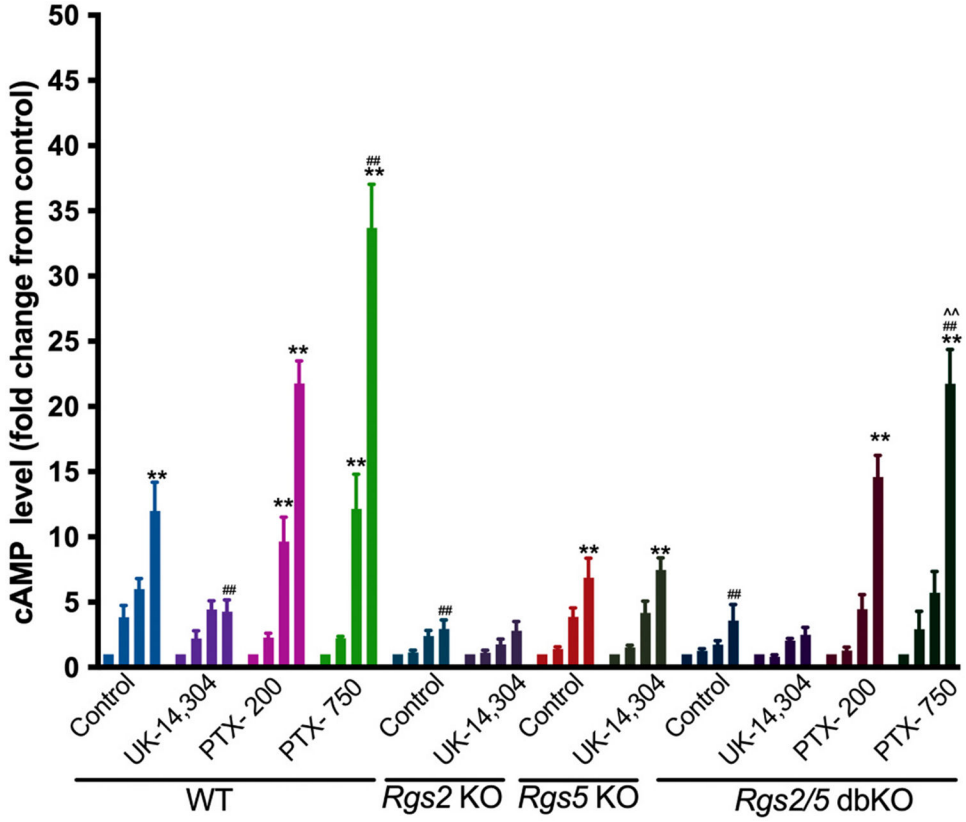

Fig. 7.

Dual loss of RGS2 and 5 increases $G_{i/o}$ activity and suppresses cAMP production in adult ventricular cardiomyocytes. Freshly isolated adult ventricular myocytes from wild type (WT, *n* = 6), *Rgs2* knockout (*Rgs2* KO, *n* = 8), *Rgs5* knockout (*Rgs5* KO, n = 8), and *Rgs2/5* double knockout (*Rgs2/5* dbKO, n = 8) male mice were stimulated with 1, 10, or 50 μM forskolin in the absence or presence of the selective α_2-adrenergic receptor agonist, UK-14,304 (1 μM). Different batches of WT and *Rgs2/5* dbKO cells were pre-incubated with 200 or 750 ng/ml of pertussis toxin (PTX) for 2 h prior to forskolin stimulation. All experiments were performed in the presence of 500 μM 3-isobutyl-1-methylxannthine (IBMX). All values are mean ± s.e.m. $^{**}P < 0.01$ vs. respective control; $^{\#\#}P < 0.01$ vs. WT treated with 50 μM forskolin; $\wedge\wedge P < 0.01$, WT cells treated with PTX and 50 μM forskolin vs. *Rgs2* dbKO cells treated with PTX and 50 μM forskolin. *P* values were obtained from 2-way ANOVA followed by Sidak post hoc tests.

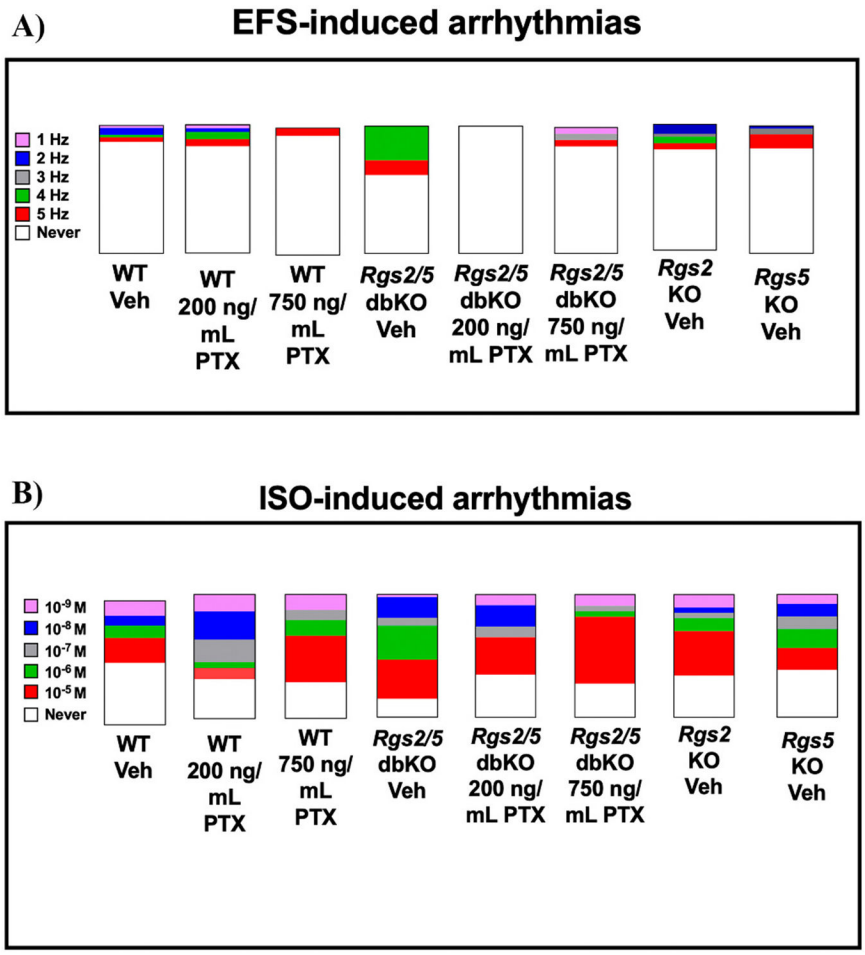

Fig. 8.

Unregulated $G_{i/o}$ activity contributes to cardiomyocyte arrhythmia resulting from the application of electrical field stimulation (EFS) or a β-adrenergic receptor (βAR) agonist. A) Stacked bar graph of percentages of male WT (*n* = 59 cells from 14 hearts), *Rgs2* KO (*n* = 25 cells from 4 hearts), *Rgs5* KO (*n* = 47 cells from 8 hearts), and *Rgs2/5* dbKO (n = 47 cells from 12 hearts) cardiomyocytes developing arrhythmia following EFS application at 1–5 Hz. B) Stacked bar graph of percentages of total number of male WT (n = 59 cells from 14 hearts) and *Rgs2/5* dbKO (n = 47 cells from 12 hearts) cardiomyocytes developing arrhythmia at 0.5 Hz, 10 V, following βAR stimulation with isoproterenol (ISO) from 10^{-9} to 10^{-5} M. For $G_{i/o}$ inhibition, cardiomyocytes were incubated with pertussis toxin (PTX, 200 or 750 ng/ml) for 2 h prior to the application of EFS or ISO.

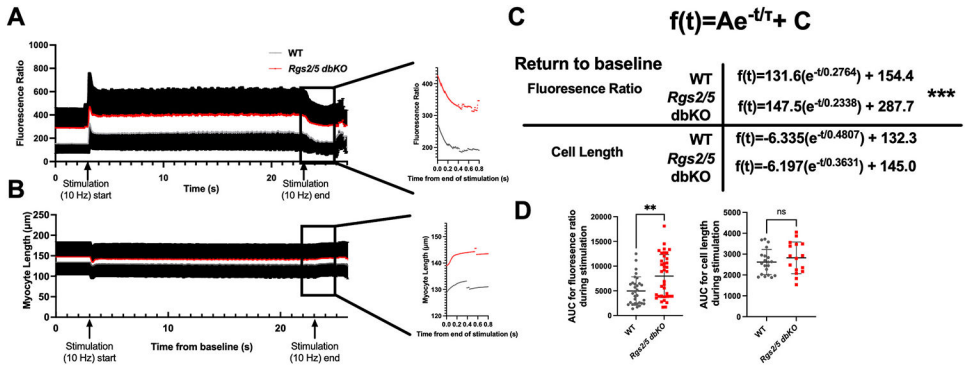

Fig. 9.

Dual deletion of RGS2 and 5 leads to exaggerated cytoplasmic Ca^{2+} rise following electrical field stimulation of adult ventricular myocytes. A, B) A time course of EFS-induced Ca^{2+} transient and contraction of ventricular myocytes from male WT (n = 40 cells from 10 hearts) and *Rgs2/5* dbKO (n = 45 cells from 12 hearts) mice. Freshly isolated ventricular myocytes were treated with thapsigargin (1 μM) to block SERCA, followed by the application of EFS at 10 Hz (10 V) for 25 s, while monitoring cytoplasmic Ca^{2+} rise and clearance by Fluo-4 fluorescence imaging. The arrows indicate the beginning and the end of EFS application. The inset shows a zoomed section (indicated by the rectangle) of the Ca^{2+} transient and contraction at the end of the EFS and during the decay of the transients and myocyte relaxation. The line graphs are representative tracings obtained by curve fitting of the data in the zoomed-in section to a first order exponential decay equation shown in 9C. D) A dot plot of area under the curve (AUC) of the fluorescence ratio-time and myocyte length-time curves for the duration of the EFS train application, indicating total accumulated cytoplasmic Ca^{2+} and force generated during the application of the EFS train. Values are mean ± s.e.m. $^{**}P < 0.01$. P values were obtained from an unpaired student's t-test.

Table 1

Hemodynamic and cardiac ECG at baseline and in response to acute isoproterenol injection and exercise-induced stress in adult male mice.

	Baseline		After ISO		After swim exercise	
	WT (n = 4)	***Rgs2/5* dbKO (n = 5)**	**WT (n = 4)**	***Rgs2/5* dbKO (n = 5)**	**WT (n = 4)**	***Rgs2/5* dbKO (n = 5)**
SBP (mmHg)	117 ± 4	134 ± 6 *	89 ± 3	88 ± 7	134 ± 7	147 ± 2
DBP (mmHg)	86 ± 6	97 ± 5	56 ± 6	50 ± 8	99 ± 1	105 ± 1
MBP (mmHg)	102 ± 5	116 ± 5 *	72 ± 4	68 ± 8	118 ± 3	127 ± 1
HR (bpm)	600 ± 36	597 ± 10	644 ± 30	576 ± 29	599 ± 14	534 ± 26
PR-I (ms)	35 ± 3	34 ± 1	32 ± 1	34 ± 1	28 ± 1	41 ± 2**
RR-I (ms)	102 ± 7	102 ± 2	93 ± 4	106 ± 7	101 ± 3	124 ± 16
QT-I (ms)	103 ± 6	102 ± 5	107 ± 5	136 ±16 *	127 ± 5	142 ± 2
ST-I (ms)	92 ± 6	91 ± 6	95 ± 5	125 ± 16 *	116 ± 5	125 ± 2
QRS duration (ms)	14 ± 1	14 ± 0	14 ± 1	15 ± 1	15 ± 1	15 ± 1
R-H (mV)	0.43 ± 0.42	0.63 ± 0.08	0.83 ± 0.21	0.73 ± 0.09	1.25 ± 0.25	1.19 ± 0.10
P-H (mV)	0.04 ± 0.01	0.06 ± 0.01	0.05 ± 0.01	0.06 ± 0.01	0.06 ± 0.01	0.10 ± 0.02
T-H (mV)	0.14 ± 0.04	0.13 ± 0.06	0.18 ± 0.04	0.04 ± 0.01**	0.28 ± 0.03	0.39 ± 0.09

Values are mean ± s.e.m. SBP, systolic blood pressure; DBP, diastolic blood pressure; MBP, mean blood pressure; HR, heart rate; xx-I, xx interval; x-H, x height.

* $P < 0.05$ vs. WT of each experimental condition. *P* values were obtained by unpaired Student's *t*-test.

J Mol Cell Cardiol. Author manuscript; available in PMC 2023 May 25.